Eur. Phys. J. D (2015) 69: 153
DOI: 10.1140/epjd/e2015-60189-1

THE EUROPEAN PHYSICAL JOURNAL D

Regular Article

Elastic scattering of low-energy electrons by CH_3CN and CH_3NC molecules

Milton M. Fujimoto[1,a], Erik V.R. de Lima[1], and Jonathan Tennyson[2]

[1] Departamento de Física, Universidade Federal do Paraná, 81531-990 Curitiba, Parana, Brazil
[2] Department of Physics and Astronomy, University College London, Gower St., London WC1E 6BT, UK

Received 19 March 2015 / Received in final form 27 April 2015
Published online 11 June 2015 – © EDP Sciences, Società Italiana di Fisica, Springer-Verlag 2015

Abstract. Rotationally-summed elastic cross sections for electrons collisions with the isomers acetonitrile and methyl isocyanide are reported. Theoretical differential and integral cross sections are calculated using the UK molecular R-matrix codes in the energy range from 1 eV to 10 eV. The dynamic interaction is represented within a static-exchange plus polarization model based on the use of an extensive orbital sets. Both molecule have a large permanent dipole moment and a Born closure procedure is used to get more reliable cross sections. These molecules show low-energy, π^* resonances at 2.4 and 2.7 eV for CH_3CN and CH_3NC, respectively; and very broad σ^* ones at about 6 eV. Our results suggest that electron collisions with CH_3CN / CH_3NC show similar properties to those found for electron collisions with HCN / HNC.

1 Introduction

Molecules containing cyanide and isocyanide groups have many different uses in chemical industries [1,2]. The CH_3CN (acetonitrile or methyl cyanide) molecule was detected in the interstellar clouds [3] and can be considered as building block for amino acids [4].

The isomers CH_3CN and CH_3NC (methyl isocyanide or isocyanomethane) have large, permanent dipole moments (>3 Debye). Closed-shell molecule molecules with permanent dipoles above a critical value of about 2 Debye can form "dipole-bound" molecular anions [5,6]. Theoretical and experimental studies have shown the existence of "dipole-bonded" anion of CH_3CN^- [7,8]. There are also studies of dissociative electron attachment (DEA) for both CH_3CN and CH_3NC in the gas phase [9–13]. Studies to understand the effect of surfaces on DEA have also been performed for CD_3CN [14] and CH_3CN [15]; in particular Bass et al. [15] demonstrated that there are some similarities between the products generated by gas phase and condensed phase DEA. However due to the different environments, the stabilization of the CH_3CN^- molecules anion states is different which changes the resonance energies, appearance energies of ions and even fragmentation patterns leading, for example to CH_2^-, which not appear in gas phase DEA.

Another issue related to electron scattering from molecules with large permanent dipole moments is the discrepancy between theoretical integral cross sections (ICS) and the measured ones. Basically, this is due on one hand to the way experimental differential cross sections (DCS) are interpolated at small and large angles [16] and, on the other hand, to the way that theorists take into account nuclear dynamics. So obtaining reliable ICS for molecules with large permanent dipole moments remains a challenge.

In this paper we report elastic integral cross sections for low-energy (below 10 eV) electron collisions with CH_3CN and CH_3NC computed using the UK molecular R-matrix codes. Shape resonance are studied using both the static exchange and the static-exchange plus polarization approach for both molecules. This paper is organized in the following sections: Section 2 gives a brief description of the R-Matrix method used and details of the calculations; Section 3 presents DCS and ICS results for CH_3CN and CH_3NC, and a comparison with available results for HCN; in the last section we present our conclusions.

2 Calculations

2.1 The R-Matrix method

In this work, R-matrix theory is used to describe electron scattering by molecules and the UK polyatomic R-matrix (UKRMol) codes [17] were employed to calculated the cross sections and quantities of interest. The R-matrix method applied to molecules is presented in detail elsewhere [18–21]. Here we present a brief overview of this method using the nuclei-fixed frame.

In the R-matrix formulation space is split into an inner and an outer region. The inner region is defined as the space inside of a sphere of radius $r = a$ in which the centre-of-mass of the molecule defines the origin of the coordinates. The radius a is chosen in order to have all electronic

[a] e-mail: milton@fisica.ufpr.br

density of the target molecule inside the sphere. In the inner region, the system is represented by a complex comprised of N electrons of the molecule plus one continuum electron, ($N + 1$ electrons). As the interactions between the scattering electron and all electrons of the molecule is strong is the inner region, it is important to consider exchange, polarization and correlation effects. The wave function inside the sphere is represented by

$$\Psi_k^{N+1}(x_1 \ldots x_{N+1}) = \mathcal{A} \sum_{ij} a_{ijk} \phi_i^N(x_1 \ldots x_N) u_{ij}(x_{N+1}) + \sum_i b_{ik} \chi_i^{N+1}(x_1 \ldots x_{N+1}) \quad (1)$$

where ϕ_i^N represents the N-electron wave function of the isolated molecule in its ith state, u_{ij} is a continuum orbital associated with the molecule in the ith state; $\mathcal{A}$ is the antisymmetrization operator due to indistinguishability of the electrons; χ_i^{N+1} is an L^2 configurations of all $N + 1$ electrons generated by placing the extra electron in one of target molecular orbitals, including virtual orbitals, obtained from a self consistent field calculation. In static exchange (SE) calculations this term is used to relax the constraint of orthogonality between the continuum orbitals and molecular orbitals of the same symmetry. a_{ijk} and b_{ik} are coefficients determined variationally by diagonalization of the Hamiltonian matrix constructed using a specially adapted code [22]. In the inner region, the continuum electron orbitals were constructed using Gaussian type orbitals (GTO) [23] for which we used up to $\ell_{\max} = 4$ which corresponds to s, p, d, f and g orbitals.

The R-matrix is constructed on the boundary and used to match the inner and outer solutions for the continuum electron. In the outer region the R-matrix is propagated to get the K-matrix and hence cross sections.

In the outer region it is not necessary to consider exchange and correlation effects, and solutions are obtained by solving a set of one-electron, coupled, second-order differential equation. As CH_3CN and CH_3NC both have large permanent dipole moments, and in order to take into account the long-range interaction, a Born closure procedure was employed. In the R-matrix method the continuum orbitals are calculated using partial waves up to $\ell_{\max}$ and the higher partial waves are included in scattering T-matrices via analytical Born T-matrices, using the rotating dipole approximation to calculate rotational motion to avoid the divergence of nuclei fixed approximation [24–26]. For this we used the code POLY-DCS [27] which performs a frame transformation from a body-fixed formulation neglecting rotational motion to a space-fixed axis system including the rotational motion [28] and then calculates rotational excitation ($J = 0 \rightarrow J' = 0, 1, 2, \ldots$) cross sections. It should be noted that rotational transitions other than those with $\Delta J = 1$ are completely dominated by short-range effects and do require any Born correction [29,30]. The converged sum of these rotationally-resolved cross sections can be compared to the experimental rotationally-unresolved cross sections. We note that it is customary, particularly for measured cross sections, to refer cross sections which are rotationally summed as "elastic".

Table 1. Equilibrium geometry data used for ground state of CH_3CN and CH_3NC. Distances in Å and angles in degrees.

parameters	CH_3CN^a	CH_3NC
R (C2-N)	1.1572	1.1446
R (X-C3)	1.4458	1.4205
R (C3-H)	1.1120	1.0796
∠ (X-Y-C3)	180.00	180.00
∠ (X-C3-H)	109.40	109.53
∠ (H-C3-H)	109.54	109.40

X = N and Y = C2 for CH_3CN and X = C2 and Y = N for CH_3NC. [a] Experimental distances from [34].

It is difficult experimentally to resolve rotational excitation, so there are only a few studies available on which tests of the above methodology can be performed. However in these cases, such as for water [31], the agreement is found to be excellent. Similarly tests between very different procedures for treating rotational excitation also show excellent agreement [32]. Furthermore, tests, again on water, have shown that rotationally-summed elastic cross sections are almost entirely independent of temperature [33] meaning that calculations based on the use of an initial $J = 0$ level, which correspond to the molecule at 0 K, should give results appropriate for other temperatures.

2.2 Calculation details

All calculations were performed using the nuclei-fixed approximation and the isolated molecules CH_3CN and CH_3NC are described in their ground state using Hartree-Fock self-consistent-field (HF-SCF) with a cc-pVTZ basis set. The molecular structures are shown in Figure 1 and the equilibrium geometry used here is given in Table 1, where we have used experimental geometry for CH_3CN [34] and for CH_3NC we have optimized the geometry using cc-pVTZ basis set in Hartree-Fock level. Both molecules have C_{3v} point group symmetry, but as C_{3v} is not implemented in the UK molecular R-matrix packages the reduced symmetry of the C_s point group was used. This gives symmetries A' and A'' but, where possible, full symmetry labels are used below. For example, for resonances of E symmetry the A' and A'' results coincide, otherwise they correspond to A_1 and A_2 symmetries in C_{3v}, respectively. Our calculations give permanent dipole moment of 4.17 D and 3.75 D which can they can be compared with the slightly lower experimental values of 3.92 D and 3.83 D [35], respectively for CH_3CN and CH_3NC. As the cross section depends approximately on the square of these dipoles, then this should lead to an overestimate of the rotationally-summed cross sections by about 13% and 4%, respectively.

For the scattering calculations, we initially employed the Quantemol-N expert system [36] to rapidly generate the inputs required by the UKRMol codes [17]; these were

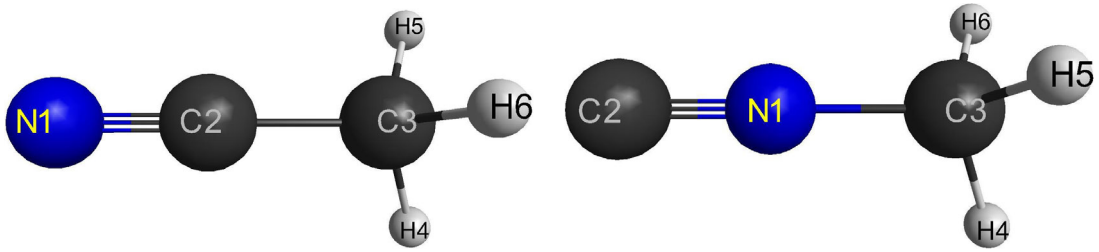

Fig. 1. Molecular structures of CH_3CN and CH_3NC.

then modified for more detailed studies, such as to include different levels of polarization. We tested R-matrix radii a from $10a_0$ to $15a_0$. Although we got similar results for the eigenphase sums, we choose $a = 11a_0$ for all final calculations as we considered that this inner region basis was both balanced and numerically stable.

To include polarization effects inside the inner region we performed a systematic study including up to 55 virtual orbitals from the SCF calculation to generate two particle, one hole $(2p,1h)$ L^2 configurations, in singlet and triplet excited target states, in the second sum of equation (1). This number of virtual orbitals is enough to converge the static-exchange (SE) calculation. To describe the continuum wave function we have used GTO with $\ell_{\max} = 4$ and the higher partial waves are included via Born correction. The rotational constants, in meV, used to calculate the rotational excitation cross sections with the program POLYDCS are $A = 0.6283846$, $B = 0.0384294$ and $C = 0.0384294$ for CH_3CN and $A = 0.6678389$, $B = 0.0424381$ and $C = 0.0424381$ for CH_3NC.

3 Results and discussion

3.1 Eigenphase sums

Before computing final cross sections, we performed a systematic study of the convergence of the eigenphase sums in both the A' and A'' symmetries (not shown). Calculations for both molecules behaved very similarly in our convergence studies. Firstly we converged scattering calculations using the static-exchange (SE) approximation: no more than 30 virtual orbitals were needed. Secondly we used these virtual orbitals to generate $(2p,1h)$ configurations to take into account polarization effects: the eigenphase sums were considered reasonably well converged using 55 virtual orbitals.

An automated procedure [37] using the Breit-Wigner formula was used to fit eigenphase sums and find final resonance positions and widths. For the CH_3CN molecule, in the SE model below 10 eV both eigenphase sums (for A' and A'') display one broad (1.3 eV wide) resonance structure near 5.0 eV. Since the SE approximation can only give shape resonances and this one is clearly doubly degenerate, we assign it as an E symmetry (π^*) shape resonance. In the SEP calculations this resonance feature moves to lower energy and becomes narrower, converging to about 2.38 eV (0.4 eV). Our SEP calculations show a new broad resonances at 6.28 eV (3.81 eV) and a narrow resonance near 8.97 eV (0.01 eV) both with A_1 symmetry, where the number in parentheses are the resonance widths. Our calculated resonance positions and widths for CH_3CN are summarized in Table 2.

Table 2. Resonance parameters for CH_3CN: Resonance symmetry in C_{3v} plus Energy (width), in eV for static exchange (SE) and static exchange plus polarization (SEP) models. The SEP calculations used 55 virtual orbitals.

SE	E 4.96(1.32)		
SEP	E 2.38(0.39)	A_1 6.28(3.81)	A_1 8.97(0.01)

Jordan and Burrow [38] used electron transmission spectroscopy (ETS) to observe a resonance near 2.8 eV which they assigned to the π^* unoccupied molecular orbital of CH_3CN. These experimental results were confirmed by Hitchcock et al. [39] who measured electron transmission (ET) spectra for CH_3CN and CH_3NC. They (Hitchcock et al. [39]) observed intense resonances at 2.82 eV and 2.81 eV corresponding to the π^* unoccupied molecular orbital, respectively for CH_3CN and CH_3NC. These authors also observed a broad and weak resonance around 6 eV for both CH_3CN and CH_3NC, which they suggested could be related to electron capture by a σ^* molecular orbital. However this assignment is not conclusive and, at this range of energy, two particle processes, such as Feshbach or core-excited shape resonances could occur as well.

An electron energy loss spectroscopy (EELS) study performed by Edard et al. [40] suggested that the low-lying shape resonance is responsible for vibrational excitation of HCN, CH_3CN and CH_3NC. Their energy loss spectra showed a lower resonant structure at 2.3 eV for HCN and near 2.9 eV for CH_3CN and CH_3NC at a scattering angle of 30 degrees. Burrow et al. [41] using ETS observed that HCN and CH_3CN displayed strong resonances at 2.26 eV and 2.8 eV in good agreement with previous works. Burrow et al. reported that their measured ET spectra for HCN and CH_3CN do not exhibited evidence for vibrational motion by the temporary anions; they also argued that the previous calculations of Jain and Norcross [42,43] for electron autodetachment of HCN^- gave a width of 1.9 eV which would correspond to a short lifetime compared with a vibrational period of the CN stretching. The short lifetime of this resonance is supported by the more recent calculations of Varambhia and Tennyson [44].

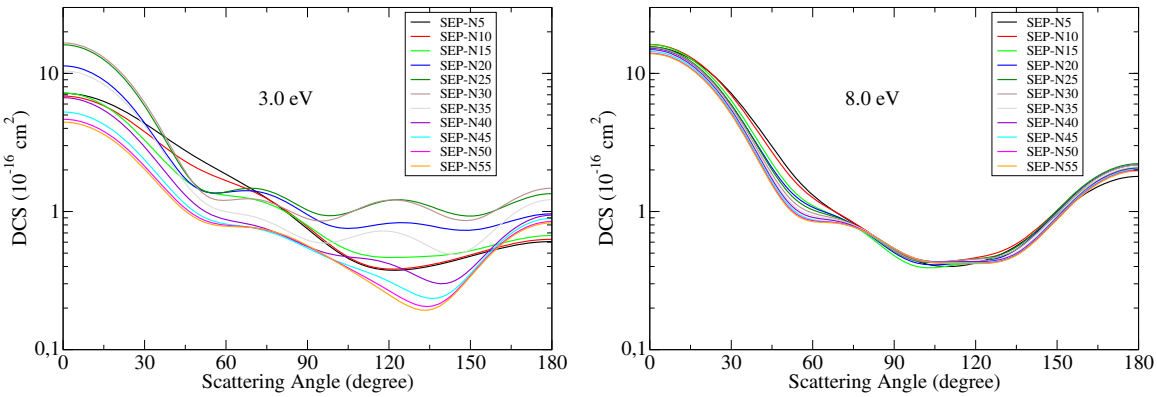

Fig. 2. Convergence of CH_3CN DCS as a function of the number of virtual orbitals (N) used in the SEP calculations with no Born correction included.

Table 3. Resonance parameters for CH_3NC: resonance symmetry in C_{3v} plus Energy (width) in eV, for static exchange (SE) and static exchange plus polarization (SEP) models. The SEP calculations used 55 virtual orbitals.

SE	E 5.53(2.05)		
SEP	E 2.70(0.89)	A_1 6.59(3.65)	A_1 9.66(0.007)

For the CH_3NC molecule, our calculated eigenphase sums showed a E-symmetry, π^* the resonance near 5.53 eV in the SE model and, after including polarization (SEP calculations), at 2.70 eV (0.89 eV). The SEP calculations also gave a broad resonance about 6.59 eV (3.65 eV) and a narrow resonance near 9.66 eV (0.007 eV), both of A_1 symmetry. These results are summarized in Table 3.

Our calculations therefore found for both isomers a broad, low-lying π^* resonance, a very broad resonance at about 6 eV which is consistent with being a σ^* shape resonance, and a high-lying, narrow A_1 symmetry resonance, which is probably a Feshbach resonance. SEP calculations are good at reproducing the properties of shape resonance, but it is probably necessary to perform close-coupling calculations to obtain reliable parameters for the Feshbach resonances.

Our calculated position of the low-lying shape resonance at 2.38 eV for CH_3CN is closer to that of HCN at 2.3 eV than the observations. On the other hand, for CH_3NC the lower resonance at 2.7 is in good agreement with available experimental results near 2.8 eV. If we compare our calculations in SE for both molecules the resonance position of CH_3CN is 0.4 eV lower than CH_3NC and this difference is maintained when we include polarization, indicating that the unoccupied π^*_{CN} orbital in CH_3CN is lower-lying than π^*_{NC} orbital in CH_3NC; similar differences are found in the measurements [38,39].

Varambhia and Tennyson [44] performed a detailed study of electron collisions with HCN and HNC using the R-Matrix method. They used correlated wave functions to represent the target and 24-state close-coupling to describe the scattering with different models of polarizations. Their results confirmed the existence of $^2\Pi$ anion shape resonance for HCN and are in good agreement with previous results. They also found an $^2\Pi$ shape resonance for HNC at a similar position to the HCN one but with a narrower width. For HCN, they also found two narrow Feshbach resonances around 7.8 eV and 8.5 eV for symmetries of $^2\Sigma^+$ and $^2\Delta$, respectively. In contract, we find that the lower resonance near 2.38 eV is narrower for CH_3CN than for CH_3NC; this seems consistent as the acetonitrile anion lies lower in energy than the methyl isocyanide anion by 0.4 eV.

3.2 Differential cross sections

In this section we present our elastic differential cross sections (DCS) in the energy range from 1 to 10 eV for both isomers. All results presented use an SEP model with 55 virtual orbitals and are Born corrected unless specified. Our systematic tests suggest that the cross sections are reasonably well converged.

Figure 2 presents the DCS result for CH_3CN at 3.0 eV (left panel) and 8 eV (right panel) to illustrate the dependence of the polarization treatment on the number of virtual orbitals. To enhance the visualization of the polarization effects we do not include the Born correction in these calculations. In SE calculations, the resonance peak is near 5.0 eV and when we include more polarization (more virtual orbitals) the resonance moves down to near 2.4 eV, so the DCS increases in the region around 2 eV. The plot at 3 eV appears to suggest that the DCS is not completely converged, but this is because the resonance position, which is near this impact energy, shifts as more polarization is included. At others energies, such as at 8 eV (right panel), far from the resonance region, we obtain good convergence for the DCS by including up to 55 virtual orbitals. The same behaviour was found to the CH_3NC (not shown).

Figure 3 compares our calculated DCS at 3 eV (left panel) and 5 eV (right panel), including polarization and Born correction, with other theoretical and of experimental results for HCN molecule. Since, to our knowledge, there are no available DCS results for either CH_3CN or CH_3NC, we compare with available data for HCN and HNC. These systems have similarities between them,

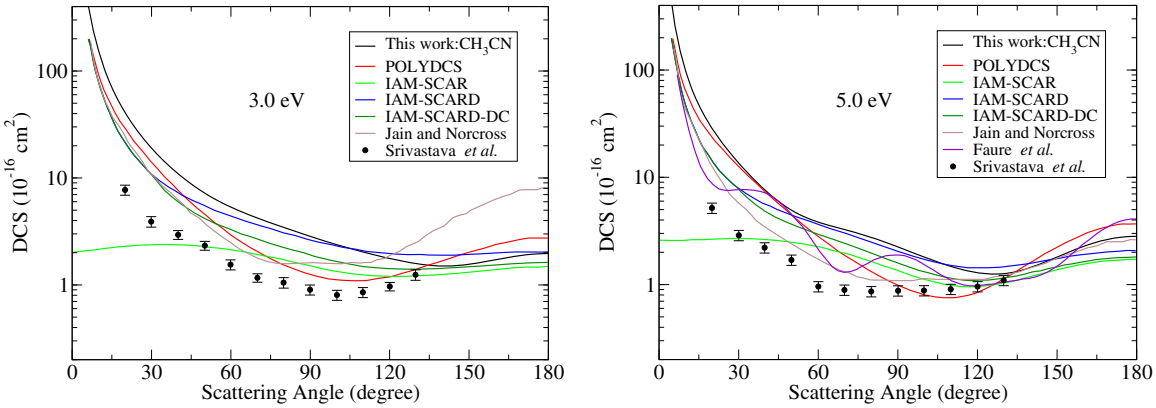

Fig. 3. Comparison of DCS for CH_3CN calculated at the SEP level, including Born correction, with available results for HCN. Impact energies are shown in the panel. (Black line) this work; results for HCN: (red line) POLYDCS [45]; (light green) IAM-SCAR (without Born correction) [45]; (blue) IAM-SCARD [45]; (dark green) IAM-SCARD-DC [45]; (brown) Jain and Norcross [42]; (purple) Faure et al. [46]; (circle) Experimental results of Srivastava et al. [47].

such as, large dipoles and shape resonances associated with the π^*_{CN} and π^*_{NC} orbitals. This comparison provides a good way to assess our new results, especially when we discuss the behaviour of the resonances. HCN is smaller than both isomers which we are studying; however, it is a polar molecule and hence displays the same divergent behaviour at forward angles due to its large permanent dipole. The DCS for CH_3CN and CH_3NC are similar, and around 5 times larger than the experimental results for HCN at the angles from 20 degrees up to 100 degrees. The theoretical results for HCN are, in general, lower than our results. We can attribute the difference in the DCS of HCN compared with that of CH_3CN and CH_3NC as being mainly due to the exchange of a H atom with a CH_3 group. Another difference observed is that DCSs for HCN at 3 eV and 5 eV display a minimum near 90°, indicating that the dominant contribution is given by *p*-partial waves, while the DCSs for both isomers show a minimum near 45° and 135° more consistent with contributions of *d*-partial waves.

Our DCS are of similar magnitude compared to theoretical results for HCN. More specifically, the results at 5 eV are closer than those at 3 eV, probably due the nearby resonance at the lower energy. At 5 eV, we can compare with the HCN results of Faure et al. [46] which were calculated with the same UKRMol codes as ours, but their calculations are more sophisticated. While we use a Hartree-Fock wave function to describe the target, they used a complete active space configuration interaction (CASCI) method improved by the use of a pseudo-natural orbital calculation. Beyond that, their scattering wave functions were represented by a close-coupling expansion including 24 target electronic states as they were interested in electronic excitation as well. Our calculation are just for a single target state with the SEP model which probably converges polarisation effects better at low energy but, of course, neglects electronic excitation. Therefore, it is not straightforward to interpret the differences observed between our results for CH_3CN and CH_3NC and those of Faure et al. for HCN, apart from the obvious fact that the molecules are different. Faure et al.'s results display more oscillations whilst our results are closer in behaviour to the calculations of Sanz et al. [45] and Jain and Norcross [42,43], the latter of which used neither a correlated wave function for the target nor a close-coupling expansion for the scattering model. At 5 eV, we have quantitative agreement with POLYDCS results [45] for forward angles up to 45°, where the long range of dipole interactions are dominant. The IAM-SCAR DCS results [45] do not show divergent behaviour at forward angles because a Born correction was not included in these calculations. We discuss below how this affects the ICS results.

Figure 4 presents a comparison between our calculated SEP-DCS for CH_3CN and CH_3NC, including Born corrections, for impact energies from 1 eV to 10 eV. The results show that when we do calculations with Born closure procedure the DCS for both molecules are very similar for angles higher than 20 degrees over the whole energy range considered. The main reason for this behaviour is probably the presence of a large dipole moment for both these molecules which implies that this long-range interaction is more important than polarization in the interaction of continuum electron and molecule.

3.3 Integral cross sections

Figure 5 compares the integral cross sections (ICS) computed including polarization effects through the 55 virtual orbitals for CH_3CN (left panel) and CH_3NC (right panel) in the energy range from 1 to 10 eV. Our systematic study shows that the ICS are reasonably well converged. To observe the behaviour of the resonance when the polarization was included we present our results without including the Born closure procedure, because the long-range dipole interactions would mask the polarization effects, since these molecules have a large permanent dipole. In our ICS results it is possible to see that the strong lower energy resonance and the peak positions for these two isomers are slightly different, the CH_3CN shows a resonance at near 2.4 eV and generates a temporary anion

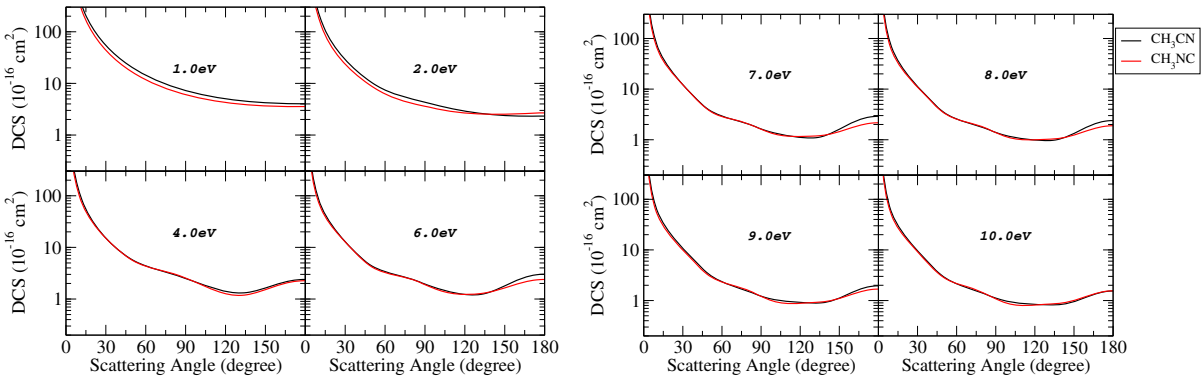

Fig. 4. Comparison of DCSs for CH_3CN and CH_3NC using Born-corrected SEP calculations. (black line) CH_3CN and (red line) CH_3NC.

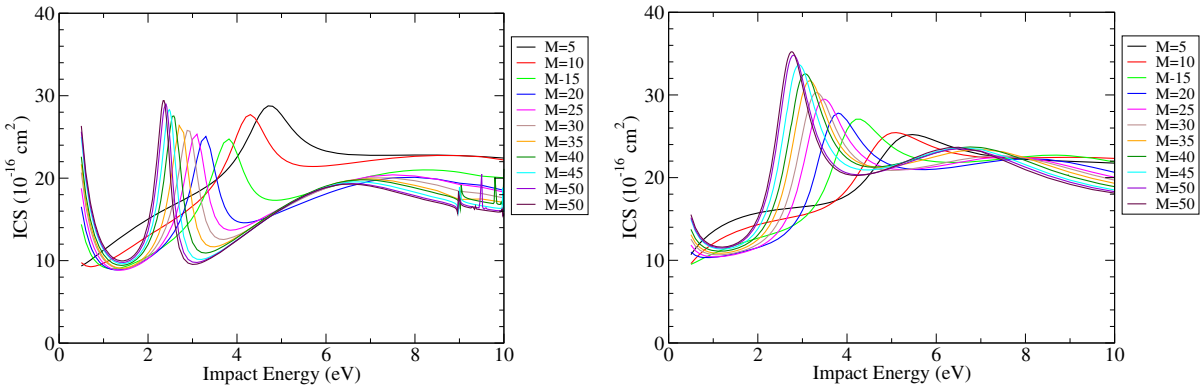

Fig. 5. Convergence of the integral cross sections for CH_3CN and CH_3NC at the SEP level, without Born corrections. The plots show the dependence on polarization effects as a function of the number of virtual orbitals, M, included in the calculation.

state approximately 0.4 eV lower than CH_3NC. The results for CH_3CN are close to those for HCN which displays a resonance near 2.3 eV. These difference in energy for two isomers can be related to the different stability for the π^*_{CN} and π^*_{NC} molecular orbitals. It is important to mention, as discussed above in Section 3.1, that previous experimental results gave the same value to the lower resonance for both isomers, near 2.9 eV. But our ICS results at the static-exchange (SE) level give the same difference of 0.4 eV in the corresponding resonance peaks, indicating that π^*_{CN} molecular orbital of CH_3CN is lies lower than π^*_{NC} of CH_3NC by about 0.4 eV even when polarization is not included. Figure 5 shows a broad structure near 6 eV for both isomers which is consistent with the ETS experimental results [39,40]. As we have pointed above, our calculations for CH_3CN predict an additional narrow resonance near 9 eV.

Figure 6 compares our ICS for CH_3CN and CH_3NC including polarization effects with 55 virtual orbitals and a Born correction in the energy range from 1 to 10 eV, with other theoretical and experimental results for HCN. A complete comparison between HCN cross sections is given by Sanz et al. [45]. A comparison of our ICS results for CH_3CN and CH_3NC with a Born correction is also given in Figure 6 and our results without Born correction in Figure 5; we can see that long-range dipole interactions dominates the ICS and are thus more important than polarization effects, due to the large permanent dipole moment for both molecules. It is also possible to observe the smooth structures due resonances in Figure 6 near 3 eV. Comparing our results with other theoretical results for HCN shows that they are similar. However, the R-matrix calculations of Faure et al. [46] were performed using a different (close-coupling) model and for a different molecule, but give ICS results (shown in Ref. [45]) close to the present one. This can be understood in terms of the dominant contribution small angle scattering to the ICS, as all of these three molecules have large dipole moments. The comparison with experimental results for HCN shows that the our and the Faure et al. ICSs are larger, by a factor of almost four, than the experimental results measured at 3 eV and 5 eV. As we have reasonable agreement with the experimental DCS in the range from 30° to 130°, the likely reason for this discrepancy can be attributed to the way of Srivastava et al. [47] extended their DCS results to forward angles. Srivastava et al. used the first Born approximation (FBA) behaviour to extrapolate the DCS to angles below 20°; there is considerable discussion in the literature about both whether the FBA underestimates cross sections for polar molecules [45,48]. In particular, Fujimoto et al. [49] showed in their study of the polar ethanol molecule that to get a reliable ICSs, it is necessary to be careful about the extrapolation method used, especially at low angles. Fujimoto et al. presented a

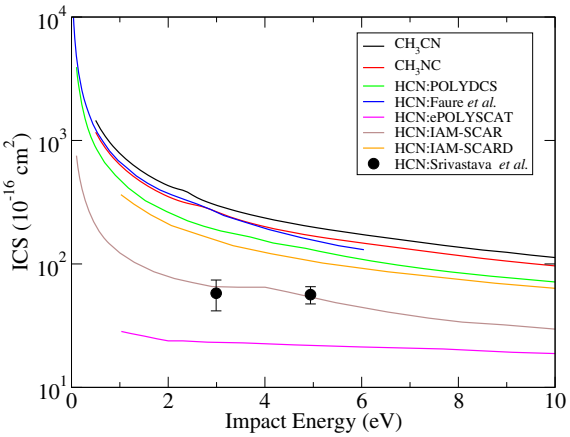

Fig. 6. Comparison between SEP-ICS for CH_3CN and CH_3NC, including Born corrections, with available ICS results for HCN. (Black line) this work for CH_3CN; (red line) this work for CH_3NC; results for HCN: (light green) POLYDCS [45]; (blue) Faure et al. [46] (ICS results shown in [45]); (magenta) ePOLYSCAT [45]; (brown) IAM-SCAR (without Born correction) [45]; (orange) IAM-SCARD [45]; (circle) experimental results of Srivastava et al. [47].

new set of "semi-empirical" ICS for ethanol using the experimental DCS measured between 20° and 130° which they extrapolated to forward and backward angles using the behaviour of calculated cross sections computed using the R-matrix method completed with a Born closure procedure. The resulting DCS was then integrated to get the ICS. This new set of results, which are a mix of theoretical and experimental data, gives good agreement with calculated cross sections, mostly due the extrapolation to lower scattering angles, which is dominated by strong long-range dipole interactions for molecules with large dipole moment.

4 Conclusions

In this article we present theoretical cross sections for CH_3CN and CH_3NC in the range 1 eV to 10 eV, calculated using the UK molecular R-Matrix programs and including polarisation and long-range dipole interactions. This work represents, to our knowledge, the first theoretical elastic DCS and ICS for these molecules. Our best results include 55 virtual orbitals in the static-exchange plus polarization (SEP) model, and can be considered converged in polarization calculations. Our study considering eigenphase sums and ICS showed us that these two isomers display resonance structure similar to those found in HCN. The low-energy resonance is stronger and narrower; they are found near 2.4 eV and 2.7 eV for CH_3CN and CH_3NC, respectively. These shape resonances occur when the continuum electron is captured by π^*_{CN} or π^*_{NC} molecular orbital or LUMO. Acetonitrile is the most stable isomer and our study shows that its temporary anion formed in the resonance is lower in energy by 0.4 eV compared to the corresponding anion of methyl isocyanide. It is possible that our model of polarization effects could overestimate this effect only for CH_3CN, since experimental results reported in the literature, suggest that the resonance positions of these two isomers are both near at 2.9 eV. However, our resonance position for acetonitrile is consistent with 2.3 eV observed for HCN.

Our calculated DCS is dominated by the long-range interactions due to the large dipole moment which results in divergent behaviour of the DCS at forward angles. At 3 eV and 5 eV, our DCSs are similar to the available results for HCN. From a comparison of our calculations without and with a Born correction, we observe that long-range interaction dominates over polarization, as our ICS results including Born corrections almost mask the presence of resonance structure. Comparing our ICS with experimental results of HCN, for impact energies of 3 eV and 5 eV, suggests that the measured ICS results are very sensitive to the method used to extrapolate them to forward angles. This comparison indicated that FBA may not be adequate to produce reliable results and that published "measured" ICS may be too low.

M.M.F. acknowledges for partial support from the Brazilian agency Conselho Nacional de Desenvolvimento Científico e Tecnológico (CNPq) and E.V.R.L. acknowledges Universidade Federal do Paraná and Fundação Araucária for scholarship.

References

1. R. Heintz, H. Zhao, X. Ouyang, G. Grandinetti, J. Cowen, K.R. Dunbar, Inorg. Chem. **38**, 144 (1999)
2. T.A. Heimer, C.A. Bignozzi, G.J. Meyer, J. Phys. Chem. **97**, 11987 (1993)
3. R.J. Habing, G.H. Macdonald, A&A **252**, 705 (1991)
4. A. Brack, *Molecular Origins of Life* (Cambridge University Press, Cambridge, 2000)
5. W.R. Garrett, J. Chem. Phys. **77**, 3666 (1982)
6. K.R. Lykke, R.D. Mead, W.C. Lineberger, Phys. Rev. Lett. **52**, 2221 (1984)
7. C.G. Bailey, C.E.H. Dessent, M.A. Johnson, J. Chem. Phys. **104**, 6976 (1996)
8. G.L. Gutsev, A.L. Sobolewski, L. Adamowicz, Chem. Phys. **196**, 1 (1995)
9. S. Tsuda, A. Yokohata, T. Umba, Bull. Chem. Soc. Jpn **43**, 3383 (1970)
10. J.A. Stockdale, F.J. Davis, R.N. Compton, C.E. Klots, J. Chem. Phys. **60**, 4279 (1974)
11. M. Heni, E. Illenberger, Int. J. Mass Spectrom. Ion Proc. **73**, 127 (1986)
12. P.R. Brooks, P.W. Harland, S.A. Harris, T. Kennair, C. Redden, J.F. Tate, J. Am. Chem. Soc. **129**, 15572 (2007)
13. W. Sailer, A. Pelc, P. Limão-Vieira, N.J. Mason, J. Limtrakul, P. Scheier, M. Probst, T.D. Märk, Chem. Phys. Lett. **381**, 216 (2003)
14. I. Ipolyi, W. Michaelis, P. Swiderek, Phys. Chem. Chem. Phys. **8**, 180 (2007)

15. A.D. Bass, J.H. Bredehöft, E. Böhler, L. Sanche, P. Swiderek, Eur. Phys. J. D **66**, 53 (2012)
16. R. Zhang, A. Faure, J. Tennyson, Phys. Scr. **80**, 015301 (2009)
17. J.M. Carr, P.G. Galiatsatos, J.D. Gorfinkiel, A.G. Harvey, M.A. Lysaght, D. Madden, Z. Maxšin, M. Plummer, J. Tennyson, H.N. Varambhia, Eur. Phys. J. D **66**, 58 (2012)
18. L.A. Morgan, C.J. Gillan, J. Tennyson, X. Chen, J. Phys. B **30**, 4087 (1997)
19. L.A. Morgan, J. Tennyson, C.J. Gillan, Comput. Phys. Commun. **114**, 120 (1998)
20. C.J. Gillan, J. Tennyson, P.G. Burke, *in Computational methods for Electron-molecule collisions*, edited by W. Huo, F.A. Gianturco (Plenum, 1995), pp. 239–254
21. J. Tennyson, Phys. Rep. **491**, 29 (2010)
22. J. Tennyson, J. Phys. B **29**, 1817 (1996)
23. A. Faure, J.D. Gorfinkiel, L.A. Morgan, J. Tennyson, Comput. Phys. Commun. **144**, 224 (2002)
24. N.T. Padial, D.W. Norcross, L.A. Collins, J. Phys. B **14**, 2901 (1981)
25. M.A. Morrison, Adv. At. Mol. Phys. **24**, 51156 (1988)
26. F.A. Gianturco, A. Jain, Phys. Rep. **143**, 347 (1986)
27. N. Sanna, F.A. Gianturco, Comput. Phys. Commun. **114**, 142 (1998)
28. D.M. Chase, Phys. Rev. **104**, 838 (1956)
29. I. Rabadan, B.K. Sarpal, J. Tennyson, J. Phys. B **31**, 2077 (1998)
30. A. Faure, J. Tennyson, Mon. Not. R. astr. Soc. **325**, 443 (2001)
31. A. Faure, J.D. Gorfinkiel, J. Tennyson, J. Phys. B **37**, 801 (2004)
32. A. Faure, V. Kokoouline, C.H. Greene, J. Tennyson, J. Phys. B **39**, 4261 (2006)
33. N.J. Mason et al., to be submitted
34. C.C. Costain, J. Chem. Phys. **29**, 864 (1958)
35. S.N. Ghosh, R. Trambarulo, W. Gordy, J. Chem. Phys. **21**, 308 (1953)
36. J. Tennyson, D.B. Brown, J.J. Munro, I. Rozum, H.N. Varambhia, N. Vinci, J. Phys.: Conf. Ser. **86**, 012001 (2007)
37. J. Tennyson, C.J. Noble, Comput. Phys. Commun. **33**, 421 (1984)
38. K.D. Jordan, P.D. Burrow, Acc. Chem. Res. **11**, 341 (1978)
39. A.P. Hitchcock, M. Tronc, A. Modelli, J. Phys. Chem. **93**, 3068 (1989)
40. F. Edard, A.P. Hitchcock, M. Tronc, J. Phys. Chem. **94**, 2768 (1990)
41. P.D. Burrow, A.E. Howard, A.R. Johnston, K.D. Jordan, J. Phys. Chem. **96**, 7570 (1992)
42. A. Jain, D.W. Norcross, Phys. Rev. A **32**, 134 (1985)
43. A. Jain, D.W. Norcross, Phys. Rev. A **84**, 739 (1986)
44. H.N. Varambhia, J. Tennyson, J. Phys. B **40**, 1211 (2007)
45. A.G. Sanz, M.C. Fuss, F. Blanco, F. Sebastianelli, F.A. Gianturco, G. García, J. Chem. Phys. **137**, 124103 (2012)
46. A. Faure, H.N. Varambhia, T. Stoecklin, J. Tennyson, Mon. Not. R. Astron. Soc. **382**, 840 (2007)
47. S.K. Srivastava, H. Tanaka, A. Chutjian, J. Chem. Phys. **69**, 1493 (1978)
48. M.H. Mittleman, R.E. von Holdt, Phys. Rev. **140**, A726 (1965)
49. M. M Fujimoto, W.J. Brigg, J. Tennyson, Eur. Phys. J. D **66**, 204 (2012)